BIOCHEMISTRY
including biophysical chemistry & molecular biology
Article

Biochemistry **2009,** *48,* 9103–9111 9103
DOI: 10.1021/bi901184r

Membrane-Induced Conformational Change of α_1-Acid Glycoprotein Characterized by Vacuum-Ultraviolet Circular Dichroism Spectroscopy†

Koichi Matsuo,‡ Hirofumi Namatame,‡ Masaki Taniguchi,‡ and Kunihiko Gekko*,§

‡*Hiroshima Synchrotron Radiation Center, Hiroshima University, Higashi-Hiroshima 739-0046, Japan, and* §*Department of Mathematical and Life Sciences, Graduate School of Science, Hiroshima University, Higashi-Hiroshima 739-8526, Japan*

Received July 11, 2009; Revised Manuscript Received August 21, 2009

ABSTRACT: The tertiary structure of α_1-acid glycoprotein (AGP) remains unresolved despite its novel function because AGP is a hard target in X-ray and NMR analyses. To elucidate the membrane-induced conformational change of AGP, the vacuum-ultraviolet circular dichroism (VUVCD) spectra of AGP and its constituent sugars were measured down to 160 nm in the presence or absence of phosphoglyceride liposome using a synchrotron-radiation VUVCD spectrophotometer. The secondary-structure contents and numbers of segments of AGP were estimated from the VUVCD spectra of the protein moiety obtained by subtracting the contributions of the glycan moiety. Further, the positions of secondary structures on the amino acid sequence were predicted by combining the VUVCD data with a neural network algorithm. These comprehensive secondary-structure analyses revealed that AGP consists of 11.4% α-helices (3 segments) and 39.9% β-strands (12 segments) in the absence of liposome (pH 4.5), which are close to the proportions in the secondary structure of native AGP (pH 7.4) predicted by homology modeling, and that it consists of 47.5% α-helices (7 segments) and 2.7% β-strands (2 segments) in the presence of liposome (pH 4.5). Detailed characterization of these α-helices of AGP bound to liposome suggested that two α-helices (residues 15−27 and 161−175) in the N- and C-terminal regions strongly interact with liposome. Most of the progesterone-binding residues of AGP were involved in the sequences transferring from β-strands to α-helices or unordered structures, which coincided with the large decrease in progesterone-binding capacity of liposome-bound AGP. These results provide the first sequence-level information on the membrane-binding mechanism and structure−function relationship of AGP.

Human α_1-acid glycoprotein (AGP)[1] is the major acute phase protein, whose concentration increases in response to systemic tissue injury, inflammation, and infection (*1*, *2*). A considerable body of studies has revealed the expression and synthesis processes of AGP (*3*), but its biological function within cells remains unclear. AGP exhibits some characteristic abilities to bind to numerous basic, acidic, and neutral drugs as well as to steroid hormones (*4*, *5*). The binding capacity of AGP for neutral drugs is known to decrease due to its interaction with biomembranes, which induces a conformational change from a β-strand-rich to an α-helix-rich structure (*6*, *7*). Therefore, this conformational change of AGP coupled with the release of drugs into the membrane or cell is considered as a protein-mediated uptake mechanism of drugs (*8*).

AGP is a polypeptide consisting of 183 amino acids with two disulfide bridges (Cys5−Cys147 and Cys72−Cys165) and five glycan chains linked to asparagine residues (Asn-15, -38, -54, -75, and -85) (*9*−*11*). The glycan chains, which comprise *N*-acetylglucosamine (GlcNAc), *N*-acetylneuraminic acid (NeuNAc), L-fucose, D-mannose, and D-galactose (*11*), account for about 40% of the total mass (36 kDa) of AGP (*12*). Since AGP is a hard target in X-ray crystallography and NMR spectroscopy, its tertiary structure is not revealed, although homology modeling predicts that it has a β-barrel-like core structure (*13*, *14*). Therefore, knowledge of the secondary structure has been a clue to understanding the membrane-binding mechanism and structure−function relationship of AGP.

The secondary structure of AGP has been investigated using circular dichroism (CD), Raman, and Fourier-transform infrared (FTIR) spectroscopy (*6*, *7*, *14*), of which CD spectroscopy is the most widely used (also for other proteins) because it is very sensitive to local peptide structures and applicable to any protein at a low concentration under various solvent conditions (*15*, *16*). Recently, Raman optical activity (*17*) and vibration CD (*18*) have also been found to provide useful information on the structure of glycoproteins due to the distinguishable spectra of peptide and sugar chromophores. However, quantitative estimates of secondary structure from these methods are not well developed, in contrast to CD spectroscopy, and no information is obtainable on the numbers of segments and the sequences of α-helices and β-strands participating in the membrane-induced conformational change of AGP.

Secondary-structure analyses by CD spectroscopy have been markedly improved by the development of programs (e.g., DSSP and Xtlsstr) for assigning the secondary structures from atomic coordinates (*19*, *20*), the advancements in software (CONTIN,

†This work was financially supported by a JSPS Research Fellowship for Young Scientists (no. 19001913 to K.M.) and by a Grant-in-Aid for Scientific Research from the Ministry of Education, Culture, Sports, Science, and Technology of Japan (no. 20550153 to K.G.).

*To whom correspondence should be addressed. Phone: +81-82-424-6481. Fax: +81-82-424-7327. E-mail: gekko@hiroshima-u.ac.jp.

[1]Abbreviations: AGP, α_1-acid glycoprotein; CD, circular dichroism; FTIR, Fourier-transform infrared; GlcNAc, *N*-acetylglucosamine; NeuNAc, *N*-acetylneuraminic acid; NN, neural network; PG, L-α-phosphatidyl-DL-glycerol; VUV, vacuum-ultraviolet; VUVCD, vacuum-ultraviolet circular dichroism.

Published on Web 08/24/2009

SELCON3, and CDSSTR) for analyzing CD spectra (*21*, *22*), and the extension of CD measurements to the vacuum-ultraviolet (VUV) region (*23*). The short-wavelength limit of CD spectroscopy can be successfully extended by using synchrotron radiation as a high-flux source of photons, which yields much more accurate data that cannot be obtained with a conventional CD spectrophotometer (*24*, *25*). Thus, synchrotron-radiation vacuum-ultraviolet circular dichroism (VUVCD) spectroscopy can estimate not only the secondary-structure contents but also the numbers of α-helix and β-strand segments (*26*−*29*). Furthermore, we have recently found that the predictive accuracy of the positions of α-helices and β-strands on the amino acid sequence can be markedly improved by combining VUVCD data with a neural network (NN) algorithm (VUVCD-NN method) (*30*, *31*). Since VUVCD spectroscopy can also detect the CD spectra of carbohydrates in the VUV region below 200 nm, it would be a powerful technique for the structural analysis of AGP by correcting the spectra with those of five glycan chains.

In the present study, to elucidate the membrane-induced conformational change of AGP, we measured the VUVCD spectra of AGP and its constituent sugars from 260 to 160 nm in the presence or absence of phosphoglyceride liposome (which is a model of the biomembrane) using a synchrotron-radiation VUVCD spectrophotometer. The contents, numbers of segments, and sequences of the secondary structures of AGP were estimated using the VUVCD spectra of the protein moiety, which were obtained by subtracting the contributions of the glycan moiety, and the VUVCD-NN method, and further the tertiary structure of native AGP was predicted by homology modeling. Based on these results, the liposome-induced conformational change of AGP is discussed in relation to its membrane-binding mechanism and structure−function relationship.

MATERIALS AND METHODS

Materials. AGP from human plasma (Cohn fraction VI) and L-α-phosphatidyl-DL-glycerol (PG) sodium salt from egg yolk were purchased from Sigma (St. Louis, MO). D-Mannose, D-galactose, L-fucose, NeuNAc, GlcNAc, and other analytical grade (>98%) chemicals were also obtained from Sigma. All of these materials were used without further purification. AGP was dissolved in 20 mM sodium phosphate buffer (pH 7.4) or in 20 mM sodium acetate buffer (pH 4.5), and the solutions were exhaustively dialyzed against the same buffer at 4 °C. The dialyzed protein solutions were centrifuged at 14000 rpm for 15 min and filtered by a membrane with a pore size of 20 μm (DISMIC 25AS020AS; ADVANTEC, Tokyo) to remove aggregates. The AGP concentration was determined by absorption measurement (V-560; Jasco) using the molar extinction coefficient of 8.93 dL $(g\ cm)^{-1}$ at 280 nm (*6*).

Liposome Preparation. Liposome of PG was prepared as described previously (*7*, *32*). PG was dissolved in chloroform, and the solvent was evaporated under a stream of nitrogen gas and then under a vacuum for at least 3 h. The PG film obtained was dispersed in 20 mM sodium acetate buffer (pH 4.5). Small unilamellar vesicles were prepared by sonication with a probe sonicator (VP-5S, Taitec) to near optical transparency, and residual multilamellar vesicles and titanium particles released from the probe were removed by centrifugation at 14000 rpm for 20 min. The average diameter of the obtained vesicles at 25 °C was estimated to be 36 nm by light-scattering measurements (99-D-50; DynaPro). The liposome vesicles were mixed with AGP in sodium acetate buffer (pH 4.5) at a final concentration of 100 μM AGP and 6 mM PG; this 1:60 molar ratio of AGP to PG ensured saturated binding of AGP to liposome (*7*). The AGP−liposome mixtures were incubated at room temperature overnight before VUVCD measurements.

VUVCD Measurements. The VUVCD spectra of AGP and its constituent sugars were measured from 260 to 160 nm under a high vacuum (10^{-4} Pa) using the VUVCD spectrophotometer constructed at beamline 15 (0.7 GeV) of the Hiroshima Synchrotron Radiation Center (HiSOR). The details of the optical devices, sample cell, and data acquisition of the spectrophotometer were described previously (*26*−*29*). The path length of the optical cell was adjusted with a Teflon spacer to 50 μm for measurements from 260 to 175 nm, and no spacer was used for measurements below 175 nm in order to reduce light absorption by water. The spectra measured without the spacer (∼1.7 μm path length) were calibrated by normalizing the ellipticity to those measured using a 50 μm spacer in the overlapping wavelength region from 260 to 175 nm. Thus obtained spectra were consistent with those measured using a conventional CD spectrophotometer (J-720W; Jasco) in the far-UV region (260−200 nm). The temperature of the cell was controlled at 25 °C using a Peltier element. All of the VUVCD spectra were recorded at protein concentrations of 0.1−0.4% and sugar concentrations of 3−10% with a 0.25 mm slit, a 16-s time constant, a 4 nm min^{-1} scan speed, and using four to nine accumulations. The ellipticity was reproducible within an error of 5%, which was mainly attributable to noise and to inaccuracy in the optical path length. The molar ellipticities of AGP with and without the glycan moiety were calculated with the average residue weight of 117.7, and those of the constituent sugars were calculated using their molecular weights.

Secondary-Structure Analysis. The secondary-structure contents and numbers of segments of AGP were analyzed using the SELCON3 program (*21*, *22*) and the VUVCD spectra down to 160 nm of the following 31 reference proteins with known X-ray structures (*28*, *29*) (their PDB codes are in parentheses): met-myoglobin (1WLA), hemoglobin (1G08), human serum albumin (1E78), cytochrome *c* (1HRC), peroxidase (1ATJ), α-lactalbumin (1F6S), lysozyme (1HEL), ribonuclease A (1FS3), insulin (4INS), lactate dehydrogenase (9LDT), glucose isomerase (1OAD), lipase (3LIP), conalbumin (1OVT), transferrin (1LFG), catalase (7CAT), subtilisin A (1SBC), α-amylase (1BAG), papain (9PAP), ovalbumin (1OVA), β-lactoglobulin (1B8E), pepsin (4PEP), trypsinogen (1TGN), α-chymotrypsinogen (2CGA), soybean trypsin inhibitor (1AVU), concanavalin A (2CTV), staphylococcal nuclease (1EY0), thioredoxin (2TRX), carbonic anhydrase (1G6V), elastase (3EST), avidin (1AVE), and xylanase (1ENX). We used these proteins, which are mostly ordinary globular proteins, in the present study because there is no such data set for glycoproteins at present. The secondary structures of these proteins in crystal form were assigned using the DSSP program (*19*). The bends were treated as turns, and the 3_{10}-helices and the single residues assigned as turns and bends were classified into unordered structures. Furthermore, the numbers of α-helix and β-strand segments were estimated by splitting them into regular (α_R and β_R) and distorted (α_D and β_D) classes, assuming that four residues per α-helix and two residues per β-strand were distorted (*22*). Thus, the protein structure was classified into six types: regular α-helices (α_R), distorted α-helices (α_D), regular β-strands (β_R), distorted β-strands (β_D), turns, and unordered structures. The root-mean-square deviation (δ) and

the Pearson correlation coefficient (r) between the X-ray and VUVCD estimates of the secondary-structure contents for 31 reference proteins were 0.058 and 0.85, respectively, indicating the high accuracy of the VUVCD estimation (*28*, *29*).

Sequence-Based Prediction of Secondary Structures. The positions of secondary structures (α-helices and β-strands) on the amino acid sequence were predicted by combining VUVCD analysis with the NN algorithm (VUVCD-NN method) (*30*). We adopted the NN algorithm developed by Jones (*33*), which predicts the position of secondary structures using evolutional sequence information based on the position-specific scoring matrices generated by the PSI-BLAST algorithm. A training data set of 607 proteins was prepared from the X-ray structures in the PDB (September 2006 version) (*34*) by eliminating the short chains (<30 residues), unidentified sequences, similar sequences ($<25\%$), and chain breaks (*30*). The secondary structures of these proteins were assigned using the DSSP program (*19*). The weights and biases of 20 amino acids for α-helices and β-strands were calculated from the secondary structures and amino acid sequences of these 607 proteins using a free simulation package (Stuttgart Neural Network Simulator, version 4.2) (*35*). Thirty of the above 31 reference proteins (excluding insulin) were used as the target proteins for the NN analysis.

The positions of α-helices and β-strands on the amino acid sequence were assigned in descending order of the α-helix and β-strand weights of the 20 amino acids until the determined numbers of α-helix and β-strand residues converged to those estimated from the VUVCD analysis. Next, the numbers of α-helix and β-strand segments estimated from the VUVCD analysis were introduced into the NN calculation until the predicted numbers of segments converged to those obtained from the VUVCD estimation. If the predicted numbers of residues and segments for α-helices and β-strands did not converge to the VUVCD estimates, the sequence alignment that minimized the difference between the two estimates was taken as the final solution. The predictive accuracy of this VUVCD-NN method was 75% for the above 30 reference proteins. The computational protocol for the VUVCD-NN method was detailed previously (*30*).

Modeling the Tertiary Structure. The model of the tertiary structure of native AGP was generated by the Modeler (version 9v6) package (*36*) in the form of non-hydrogen atoms according to the method (Modeler version 6) of Kopecký et al. (*14*). The template was constructed with the three-dimensional structures of four members of the lipocalin family (1EW3, 1EPA, 1QQS, and 1A3Y) that have been revealed by X-ray crystallography. The obtained model was subjected to an optimization protocol available in the Modeler package. Finally, the model of the tertiary structure was checked with ProCheck (*37*).

RESULTS

The VUVCD spectra of AGP were measured from 260 to 160 nm using a VUVCD spectrophotometer in the native (N) state at pH 7.4, partially acid-denatured (PA) state at pH 4.5, and liposome-binding (I) state at pH 4.5. The VUVCD spectra of the constituent sugars of glycan chains were also measured in the same wavelength range to estimate the contribution of the glycan moiety to the VUVCD spectra of AGP. All of the VUVCD spectra were constant within the experimental error (5%) during the data-acquisition period (about 2 h), indicating that the samples were not damaged by the synchrotron radiation of our small storage ring (0.7 GeV). Thus, the obtained VUVCD spectra are available for investigating the liposome-induced conformational change of AGP.

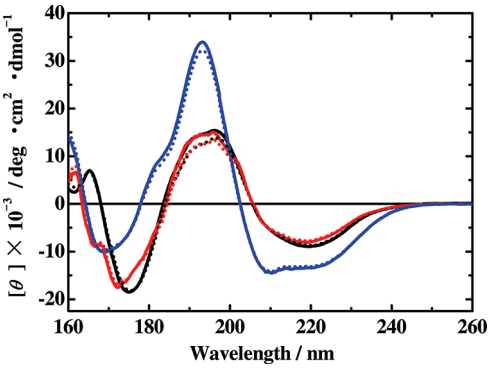

FIGURE 1: VUVCD spectra of AGP in the N-, PA-, and I-states at 25 °C (black, red, and blue lines, respectively). Dotted lines show spectra of the protein moiety obtained by subtracting spectra of the glycan moiety (inset of Figure 2) from AGP spectra. A cell with a path length of 50 μm was used for the measurements from 260 to 175 nm, and no spacer was used below 175 nm. All spectra were recorded with a 1.0 mm slit, a 16 s time constant, a 4 nm min^{-1} scan speed, and using four to nine accumulations.

VUVCD Spectra of AGP. Figure 1 shows the VUVCD spectra of AGP in the N-, PA-, and I-states. The N-state exhibited the VUVCD spectrum characteristic of β-strand-rich proteins, with two positive peaks around 195 and 165 nm, and two negative peaks at 220 and 175 nm (*28*, *29*). The negative peak at 220 nm was also observed in far-UV CD spectroscopy (*7*). A similar VUVCD spectrum was observed in the PA-state although its peaks were blue shifted by 3−5 nm in the VUV region below 180 nm, indicating that the secondary structures of AGP were only slightly modified by lowering the pH from 7.4 to 4.5. On the other hand, AGP showed a very different VUVCD spectrum in the presence of liposome (I-state), with three negative peaks at 222, 208, and 170 nm, a positive peak at 195 nm, and a shoulder around 175 nm, which are characteristic of α-helix-rich proteins (*28*, *29*). Since no CD signal due to coexisting liposome was observed between 260 and 160 nm, these results clearly demonstrate that the conformation of AGP changed from a β-strand-rich to an α-helix-rich structure by interacting with liposome. Such structural changes have also been detected by far-UV CD spectroscopy down to 200 nm (*7*), but the VUVCD spectra provide the accurate contents and segment numbers of secondary structures of AGP by extending the short-wavelength limit to 160 nm. However, in contrast to this advantage, it should be noted that the sugar moiety has a greater influence on the VUVCD spectra of AGP than on its far-UV CD spectra, which must be taken into account in the secondary-structure analysis.

VUVCD Spectra of Constituent Sugars. Figure 2 shows the VUVCD spectra of the constituent sugars fucose, galactose, mannose, GlcNAc, and NeuNAc at pH 7.4. Mannose exhibited a positive peak at 168 nm, and fucose and galactose showed two positive and two negative peaks, respectively, below 190 nm. These peaks in the VUV region are mainly caused by n−σ* transitions of ring oxygen (*38*). GlcNAc showed a negative peak at 210 nm and a positive peak at 177 nm, whereas NeuNAc showed a positive peak at 195 nm and a negative peak at 172 nm although the spectra of both sugars above 185 nm were similar to the reported ones (*39*). These CD peaks are attributable to the n−π* and π−π* transitions of the acetamido group and the

n−σ* transitions of ring oxygen (*38*, *40*, *41*). The VUVCD spectra of these sugars were also measured at pH 4.5, but only NeuNAc with an acidic (carboxyl) group showed a pH dependence with a slightly decreased peak intensity at 172 nm (Figure 2).

VUVCD Spectra of the AGP Glycan Moiety. The VUVCD spectrum of the glycan moiety of AGP was calculated by a linear summation of the CD spectra of all the constituent sugars (Figure 2) using their weight proportions in the glycan chains: 0.6% fucose, 8.5% galactose, 7.4% mannose, 16.27% GlcNAc, and 10.03% NeuNAc, which correspond to 1.5, 18.9, 16.4, 29.9, and 14.7 mol/mol of glycan chain, respectively (*11*). Contributions of glycosidic linkages between the constituent sugars were not considered because there are no VUVCD data for the various types of glycosidic linkages. However, these contributions would not be particularly significant because the CD spectrum from 260 to 185 nm of the refined glycan chains of AGP is known to be very similar to that calculated by the linear summation of the CD spectra of all the constituent sugars (*39*). The inset of Figure 2 shows the VUVCD spectrum of the glycan moiety per molar ellipticity unit calculated using the average residue weight of the glycan chains. There are two negative peaks at 212 and 172 nm and two positive peaks at 190 and 167 nm in the calculated spectrum of the glycan moiety at pH 7.4. The CD intensity is very large at 190 nm due mainly to the positive CD bands of GlcNAc and NeuNAc, while it is very small in the VUV region below 180 nm because the positive CD bands of mannose and GlcNAc are compensated by the large negative CD bands of galactose and NeuNAc. There was a small difference in the spectrum of the glycan moiety below 180 nm for pH values of 7.4 and 4.5 due to the pH dependence of the NeuNAc spectrum (inset of Figure 2).

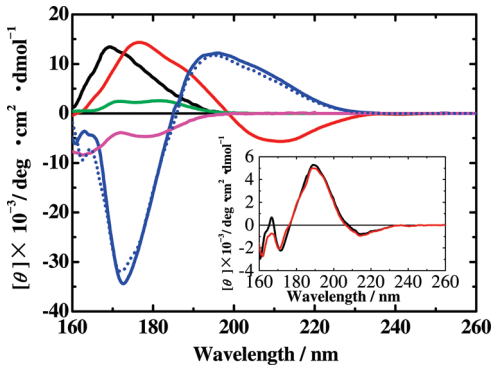

FIGURE 2: VUVCD spectra of the constituent sugars of AGP in water at 25 °C. Solid lines: mannose (black), fucose (green), galactose (pink), GlcNAc (red), and NeuNAc (blue) at pH 7.4. Blue dotted line: NeuNAc at pH 4.5. The inset shows the VUVCD spectra of the glycan moiety calculated from those of the constituent sugars at pH values of 7.4 (black) and 4.5 (red). The optical cell and the data acquisition were the same as those for Figure 1.

VUVCD Spectra of the AGP Protein Moiety. The VUVCD spectra of the protein moiety of AGP were obtained by subtracting the spectra of the glycan chain (inset of Figure 2) from the observed spectra of AGP in the N-, PA-, and I-states (Figure 1), based on the weight proportion of protein and glycan in AGP (*11*) and the pH dependence of the spectra. First, the AGP spectrum in Figure 1 was converted to the ellipticity unit per total molecular weight of the protein and glycan moieties. Second, the CD spectrum of the glycan chain in Figure 2 was converted to the ellipticity unit per total molecular weight of the glycan chain, and the obtained ellipticities were subtracted from the ellipticities of the AGP spectrum. In this way the obtained spectra of the protein moiety of AGP were divided by the number of amino acid residues (183) to convert the spectra to the molar ellipticity unit. As shown in Figure 1, the protein moiety exhibited a smaller CD intensity than AGP between 200 and 180 nm in all the N-, PA-, and I-states, but no substantial differences were observed in other wavelength regions. The decrease in CD intensity at 193 nm amounts to 3000 deg cm^2 dmol^{-1}, which corresponds to about 10% and 20% of the intensities of AGP spectra in the I- and N-states, respectively, which cannot be neglected in the secondary-structure estimation of AGP.

Contents and Segment Numbers of Secondary Structures. The contents of secondary structures (α-helices, β-strands, turns, and unordered structures) of AGP in the N-, PA-, and I-states were estimated using the SELCON3 program and the VUVCD spectra of AGP down to 160 nm with and without the glycan moiety. The results of the estimation are listed in Table 1 with those of native AGP estimated by FTIR and Raman spectroscopy (*19*).

The numbers of α-helix and β-strand segments have previously been estimated from the CD spectra using two methods: (1) Pancoska et al. (*42*) used a matrix descriptor of secondary-structure segments for the NN-based analysis of proteins, and (2) Sreerama et al. (*22*) estimated the numbers of segments from the distorted residues of α-helices and β-strands, assuming that on average there were four and two distorted residues per α-helix and β-strand, respectively. The results of these two analyses are comparable, and hence we used the method of

Table 1: Secondary-Structure Contents and Segment Numbers of AGP with or without Glycan Chains in Native (N), Partially Acid-Denatured (PA), and Liposome-Binding (I) States[a]

		α-helices		β-strands			
states		content (%)	no.	content (%)	no.	turns (%)	unordered structures (%)
N	+glycan	16.5	4	34.8	11	20.6	31.6
	−glycan	14.4 (14.2)	3 (3)	37.7 (37.7)	10 (11)	19.3	28.8
	Modeler	11.5	3	36.6	10	23.5	28.4
	FTIR[b]	12		37		28	25
	Raman[b]	14		42		20	28
PA	+glycan	14.2	3	38.1	11	21.0	29.6
	−glycan	11.4 (11.4)	3 (3)	39.7 (39.9)	11 (12)	22.9	28.7
I	+glycan	50.8	8	7.3	3	18.2	26.1
	−glycan	49.9 (47.5)	8 (7)	5.6 (2.7)	2 (2)	19.3	25.4

[a]The values in parentheses represent the results of VUVCD-NN analysis (see the text). [b]Taken from Kopecky et al. (*14*).

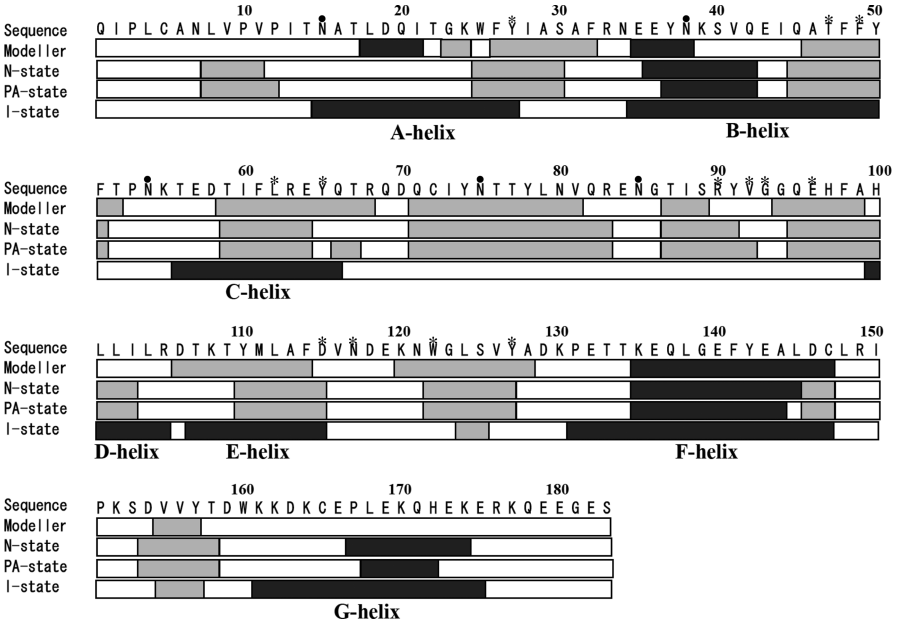

FIGURE 3: Sequence-based secondary structures of AGP in the N-, PA, and I-states predicted by the VUVCD-NN method. The sequence of native AGP predicted by homology modeling (Modeler package) is indicated on the top line. The α-helices, β-strands, and others are shown in black, gray, and white, respectively. The residues marked with filled circles (●) and asterisks (*) correspond to the glycan- and ligand-binding sites, respectively.

Sreerama et al. (*22*). The estimated numbers of α-helix and β-strand segments are listed in Table 1.

Sequence-Based Prediction of Secondary Structures. CD or VUVCD spectroscopy itself in principle yields no information on the sequences of the secondary structures, and hence an algorithm exploiting the correlations between the X-ray structures and amino acid sequences of many proteins is necessary for the sequence-based prediction of secondary structures (α-helices, β-strands, and others). A classical method of Chou and Fasman was the first used to predict the position of secondary structures of AGP (*39*), but various types of NN algorithm with much higher accuracy are currently available (*33*, *43*−*45*). In the present study, we used the NN algorithm of Jones (*33*) due to the technical convenience of combining it with VUVCD data. Since no propensity data of the 20 amino acids are available for the secondary-structure elements of nonnative proteins, the sequences of the secondary structures of AGP in the PA- and I-states as well as the N-state were predicted by constraining the NN calculation with the propensity data for native proteins and using the contents and segment numbers of α-helices and β-strands obtained from the VUVCD spectra (*31*).

The predicted numbers of α-helix and β-strand segments in the N-, PA-, and I-states are listed in Table 1, and their positions are depicted on the amino acid sequence in Figure 3. In this prediction, the turns and unordered structures estimated by the SELCON3 program were assigned into others. Native AGP includes 11 β-strands and 3 α-helices, while liposome-bound AGP consists of 7 α-helices and 2 β-strands. The numbers of segments thus predicted at the sequence level did not necessarily agree with those predicted from the VUVCD data because the sequence-alignment minimization was performed in the VUVCD-NN method (see Materials and Methods section).

Model of the Tertiary Structure. The model of the tertiary structure of native AGP constructed by the Modeler package is shown in Figure 4. The obtained model showed a high stereochemistry quality as revealed by ProCheck (*37*): the torsion

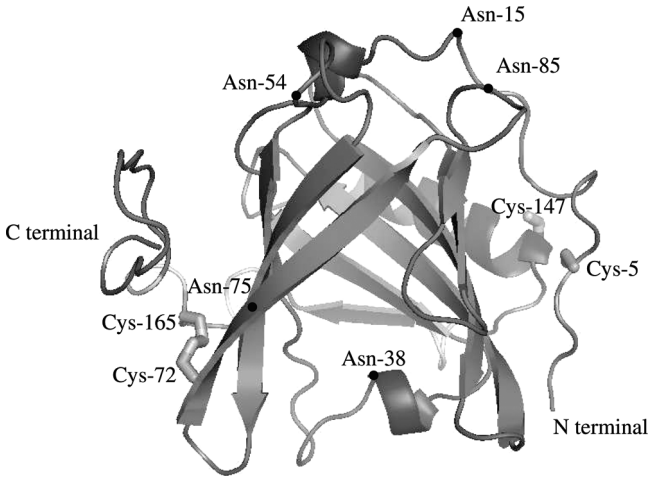

FIGURE 4: Speculative ribbon model of the native structure of AGP constructed by the Modeler package. AGP has a β-barrel-like conformation comprising 10 antiparallel β-strands and 3 α-helices. The glycan-binding residues are marked with filled circles (●).

angles of 87% of the residues had values within the most favored regions and no residues were found in disallowed regions, and the overall *g*-factor, which is a measure of deviation of a given residue from the Ramachandran plot, was −0.18. AGP folded as a highly symmetrical β-protein comprising 10 antiparallel β-strands and 3 α-helices. Our model is essentially similar to that of Kopecký et al. (*14*), with the number of β-strands (eight in their model) and the C-terminal loop region probably differing due to the different Modeler package used. The sulfur atoms of Cys72 and Cys165 were separated by 2.02 Å, as available for forming the disulfide bridge, but those of Cys5 and Cys147 were separated by 6.18 Å. The sequences of α-helices and β-strands estimated from this model are presented in Figure 3, and the contents and numbers of segments calculated from the sequences are listed in Table 1 to allow comparison with the results from the VUVCD-NN method.

DISCUSSION

The VUVCD spectra of AGP and its constituent sugars (Figures 1 and 2) evidently provide detailed information on the secondary structures, in term of not only the contents and numbers of segments (Table 1) but also their positions on the amino acid sequence (Figure 4). These results allow us to discuss the membrane-interaction mechanism and the structure−function relationship of AGP at the sequence level. However, we first discuss the characteristics of the predicted structures of AGP in the native, mildly acidic, and liposome-binding states.

Effect of Glycan Moiety on the Secondary-Structure Estimation. The effect of the glycan moiety of AGP has not been taken into consideration quantitatively in the secondary-structure estimation by far-UV CD spectroscopy, although its contribution has been shown to be negligible (*39*). VUVCD spectroscopy allows us to detect the CD spectra of the glycan moiety (constituent sugars) and analyze the secondary structures more accurately by subtracting them from the measured AGP spectra (Figures 1 and 2). As indicated in Table 1, there are small but nonnegligible differences in the secondary-structure contents determined from the VUVCD spectra with and without the contribution of the glycan chain. Evidently, the results for native AGP obtained from the VUVCD spectra without the glycan moiety are close to those from FTIR and Raman spectroscopy (*14*) in which the spectra of peptide and sugar are distinguishable (Table 1). This finding demonstrates that the secondary structures of AGP can be accurately evaluated by subtracting the contribution of the glycan moiety from the VUVCD spectra of AGP, and hence the results from the VUVCD spectra of the protein moiety are considered in the discussion below.

Secondary and Tertiary Structures of AGP in the N-State. As indicated in Table 1, native AGP consists of 37.7% β-strands (ten segments) and 14.4% α-helices (three segments). These results clearly indicate that AGP is a β-strand-rich protein in the N-state, as previously predicted by other studies (*14*, *30*, *38*). According to the VUVCD-NN analysis (Figure 3), the 3 α-helices are assigned as residues 36−42, 135−145, and 167−174 and the 11 β-strands as residues 8−11, 25−30, 45−51, 59−64, 71−83, 87−91, 95−103, 110−115, 122−127, 146−147, and 154−158. To confirm these results of SELCON3 and VUVCD-NN analyses, we further constructed the tertiary structure of native AGP using the Modeler package (Figure 4). The obtained model indicated 11.5% α-helices (3 segments) and 36.6% β-strands (10 segments), which were consistent with the results obtained from VUVCD data (Table 1). The amino acid sequence of 51.4% in this model agreed with that from the VUVCD-NN method, and two of three α-helices located at the similar corresponding positions on the sequence in both methods (Figure 3). These results indicate that the VUVCD data and homology modeling are complementary and useful for understanding the conformational change and the structure−function relationship of AGP, although elucidation of the precise three-dimensional structure must await X-ray or NMR analysis.

Secondary Structure of AGP in Mildly Acidic Solution. An important characteristic of AGP in mildly acidic solution (PA-state) is its liposome-binding ability, which is not given to the N-state although both states retain the ligand-binding ability (*7*). This suggests that there are some structural differences between the two states, but only minor differences were observed in the secondary structures obtained from the VUVCD spectra (Table 1): the α-helix content decreased from 14.4% to 11.4% without affecting the number of segments, and the β-strand content increased from 37.7% to 39.7% as the number of segments increased from 10 to 11. The VUVCD-NN analysis also showed that α-helices and β-strands are located at similar corresponding positions on the sequence in both the N- and PA-states, although an additional short β-strand (residues 66−67) is formed in the PA-state (Figure 3). These changes in the secondary structure would be too small to affect the ligand-binding capacity of AGP. On the other hand, Nishi et al. found significant changes in the fluorescence spectra of the tryptophan residues of AGP and the added probe, 1-anilinonaphthalene-8-sulfonic acid, in the two states (*7*). Thus, AGP has a unique structure in the PA-state (pH 4.5), with the secondary structure remaining almost intact and the tertiary structure being modified for binding of AGP with the membrane, probably due to the hydrophobic interaction.

Secondary Structure of Liposome-Bound AGP. When AGP binds to liposome, its α-helix content increases from 11.4% (3 segments) to 49.9% (8 segments), and its β-strand content decreases from 39.7% (11 segments) to 5.6% (2 segments) (Table 1). Thus, liposome induces a conformational change of AGP from a β-strand-rich to an α-helix-rich form with no accompanying changes in the contents of turns and unordered structures. According to the VUVCD-NN analysis, the seven α-helices of liposome-bound AGP are assigned as residues 15−27, 35−50, 56−66, 100−105, 107−115, 131−147, and 161−175, which are denoted as A-, B-, C-, D-, E-, E-, and G-helices, respectively, and the two β-strands are assigned as residues 124−125 and 155−157 (Figure 3). B-, F-, and G-helices, which comprise about four turns, are formed in the extended regions of three α-helices existing in the PA-state, but other short helices are newly formed by replacing the unordered and β-strand residues. Two β-strands (residues 124−125 and 155−157) are retained around the center of the corresponding β-strands formed in the N- and PA-states, suggesting that these two β-strands make an antiparallel β-sheet in the I-state. At present it is unclear whether the secondary-structure formation of AGP is affected by five glycan chains linked to Asn-15, -38, -54, -75, and -85, which are localized in the N-terminal region. Judging from the long loop over residues 67−99, two glycan chains linked to Asn-75 and Asn-85 in the loop may inhibit the secondary-structure formation on liposome due to steric or electrostatic repulsion because the two Asn residues are nearest on the sequence among the five.

Interaction Mechanism between AGP and Liposome. It is known that the protein−membrane interaction is mainly caused by electrostatic interactions between the anionic head groups of lipids and the positively charged residues of the protein and subsequent insertion of some hydrophobic groups of the protein into the membrane (*46*). The pH decrease at the membrane surface due to the membrane potential may also mediate interaction between the protein and membrane (*47*, *48*). The depression of the interaction between AGP and membrane by the addition of salts (*7*) and the enhancement of helix formation of AGP by exposure to more hydrophobic alcohols (*49*) indicate that both electrostatic and hydrophobic interactions participate in the AGP−membrane interaction. However, the interaction mechanism remains unclear because there is only limited information on the regions involved in the interaction between AGP and the membrane.

A crucial issue is whether AGP interacts on the membrane surface or passes through the membrane as found for typical

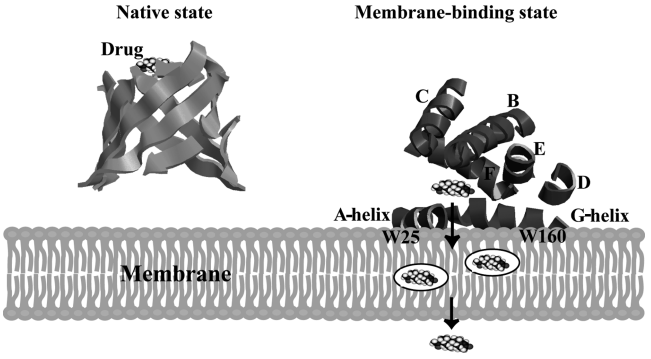

FIGURE 5: Speculative model of the membrane-binding mechanism and structure−function relationship of AGP. Positively charged AGP with ligand is drawn close to the anionic membrane surface by an electrostatic interaction. W25 and W160 are trapped in the membrane by hydrophobic interaction, forming A- and G-helices in contact with the membrane surface and subsequently B-, C-, D-, E-, and F-helices, accompanied by the release of ligand into the membrane.

membrane proteins. Therefore, the membrane-binding regions of AGP were searched using the programs PHDhtm (*50*) and SOSUI (*51*). No region that passed through the membrane was found on the sequence of AGP, suggesting that the AGP−membrane interaction occurs on the membrane surface. Therefore, we examined the characteristics of each helix in liposome-bound AGP to address the binding sites and topology of AGP on the membrane surface. The net charges of A-, B-, C-, D-, E-, F-, and G-helices were calculated to be 0, −2, −2, +2, 0, −4, and +1, respectively, based on the numbers of acidic (Asp and Glu) and basic (Lys, Arg, and His) residues in each helix segment. These net charges would be slightly increased because Asp and Glu residues (with pK_a values of about 4) are not completely ionized at pH 4.5. Therefore, anionic membrane surface would be electrostatically attractive to A-, D-, E-, and G-helices but repulsive for B-, C-, and F-helices.

In addition to electrostatic interaction, hydrophobic interaction with the membrane can be expected for some helices. According to the Helical Wheel Drawing Program (*52*), B-, E-, and F-helices were assigned as amphiphilic, indicating that the localized nonpolar surface could interact with the hydrophobic moiety of the membrane, although the extent may be reduced in B- and F-helices (with negative net charges) due to electrostatic repulsion. A-helix has a unique structure in which five nonpolar residues (A16, Y27, L18, I21, and W25) and a cationic residue K24 are located on one side of the helix and an anionic residue D19 and a sugar-linkage residue N15 are located on the other side. Since W25 and W160 are known to interact with liposome (*7*), A-helix involving W25 is a candidate site for interaction between AGP and the membrane. A stronger candidate is G-helix because W160 together with the N-terminal K161 and K162 of the helix could be a linker involved in binding with the membrane and, further, protonation of H172 plays an important role in α-helix formation when bound to the membrane (*53*). However, G-helix would not be buried deep in the membrane because it is linked to the long loop (residues 67−99) by a disulfide bridge between C72 and C165. Based on these characteristics of the binding sites, the AGP−membrane interaction mechanism is speculated as follows (Figure 5): (1) positively charged AGP is drawn close to the anionic membrane surface by an electrostatic interaction, and (2) W25 and W160 are trapped in the membrane by hydrophobic interaction, forming A- and G-helices in contact with the membrane surface followed by the formation of other helices. Although this speculative interaction mechanism is difficult to confirm experimentally at present, mass spectrometry of hydrogen−deuterium exchange coupled with protease digestion might be useful for examining such a weak or diffused binding and the topology of α-helices on the membrane surface, because this method provides useful information on protein dynamics at the sequence level (*54*). Additional techniques such as fluorescence quenching, surface-polarized IR, and fluorescence polarization would also be available for elucidating a more detailed interaction mechanism between AGP and liposome.

Structure−Function Relationship of AGP. The biological functions of AGP are unknown, but its ligand-binding activity has been commonly observed, particularly for therapeutic drugs (*9*). It is well-known that AGP releases progesterone upon interaction with reverse micelles and liposomes, with this being closely related to the conformational change of AGP (*6*, *7*). Therefore, this hormone-binding system would be a useful model for understanding the structure−function relationship of AGP and the transport mechanism of a hormone and drug *in vivo*. The progesterone-binding sites of AGP have been revealed using both experimental and theoretical approaches (*4*, *14*). Docking simulations using the program AutoDock (*14*) suggested that 20 progesterone-binding sites of AGP comprise 13 amino acid residues (Y27, T47, F49, L62, Y65, R90, V92, G93, E96, D115, N117, W122, and Y127). As seen in Figure 3, 10 of these residues are on the β-strands in the PA-state, which change to A-, B-, C-, and E-helices or unordered structures in the presence of liposome (I-state). Such a drastic conformational change of AGP would break the stereostructure of the binding sites, thereby markedly reducing the binding capacity for progesterone. However, ultrafiltration experiments have revealed that only about 20% of progesterone bound to AGP is released as the free species (*7*), which suggests that most of the released progesterone would penetrate into liposome because a new progesterone-binding pocket is hardly formed in liposome-bound AGP (Figure 5). This mechanism would be realized not only for progesterone but also for any other hormones and drugs of AGP because the liposome-induced conformational change of AGP is a wide-area event that involves breaking the binding sites of various ligands, thus leading to a general protein-mediated uptake mechanism of drugs.

CONCLUSIONS

This study applied VUVCD spectroscopy to characterize the secondary structures of AGP in the native, mildly acidic, and liposome-binding states. The comprehensive analysis of the contents, numbers of segments, and sequences of the secondary structures, together with homology modeling, revealed for the first time the liposome-induced conformational change of AGP from a β-strand-rich to an α-helix-rich form at the amino acid sequence level. These results provide important information for understanding the membrane-binding mechanism and the structure−function relationship of AGP, which are more generally related to the protein-mediated uptake and transport mechanisms of hormones and drugs. VUVCD spectroscopy coupled with an NN and homology modeling is a powerful tool in structural biology of proteins, especially for hard targets in X-ray and NMR analyses.

ACKNOWLEDGMENT

The authors thank Professor Shin-ichi Tate of Hiroshima University for helpful discussions.

REFERENCES

1. Kushner, I. (1982) The phenomenon of the acute phase response. *Ann. N.Y. Acad. Sci. 389*, 39–48.
2. Fey, G. H., and Fuller, G. M. (1987) Regulation of acute phase gene expression by inflammatory mediators. *Mol. Biol. Med. 4*, 323–338.
3. Fournier, T., Medjoubi, N. N., and Porquet, D. (2000) Alpha-1-acid glycoprotein. *Biochim. Biophys. Acta 1482*, 157–171.
4. Matsumoto, K., Sukimoto, K., Nishi, K., Maruyama, T., Suenaga, A., and Otagiri, M. (2002) Characterization of ligand binding sites on the alpha1-acid glycoprotein in humans, bovines and dogs. *Drug Metab. Pharmacokinet. 17*, 300–306.
5. Ganguly, M., Carnighan, R. H., and Westphal, U. (1967) Steroid-protein interactions. XIV. Interaction between human alpha 1-acid glycoprotein and progesterone. *Biochemistry 6*, 2803–2814.
6. Nishi, K., Sakai, N., Komine, Y., Maruyama, T., Halsall, H. B., and Otagiri, M. (2002) Structural and drug-binding properties of alpha(1)-acid glycoprotein in reverse micelles. *Biochim. Biophys. Acta 1601*, 185–191.
7. Nishi, K., Maruyama, T., Halsall, H. B., Handa, T., and Otagiri, M. (2004) Binding of alpha1-acid glycoprotein to membrane results in a unique structural change and ligand release. *Biochemistry 43*, 10513–10519.
8. Weisiger, R., Gollan, J., and Ockner, R. (1981) Receptor for albumin on the liver cell surface may mediate uptake of fatty acids and other albumin-bound substances. *Science 211*, 1048–1051.
9. Schmid, K., Kaufmann, H., Isemura, S., Bauer, F., Emura, J., Motoyama, T., Ishiguro, M., and Nanno, S. (1973) Structure of alpha1-acid glycoprotein. Complete amino acid sequence, multiple amino acid substitutions, and homology with the immunoglobulins. *Biochemistry 12*, 2711–2724.
10. Hatcher, V. B., and Jeanloz, R. W. (1973) The use of glycosidases in the structure elucidation of the carbohydrate chains of alpha1-acid glycoprotein from human plasma and cervical mucin from Macaca Radiata. *Colloq. Int. Centre Nat. Rech. Sci. 221*, 329–338.
11. Bayard, B., and Fournet, B. (1976) Hydrazinolysis and nitrous acid deamination of the carbohydrate moiety of alpha1-acid glycoprotein. *Carbohydr. Res. 46*, 75–86.
12. Halsall, H. B., Austin, R. C., Dage, J. L., Sun, H., and Schlueter, K. T. (2000) Structural aspects of alpha1-acid glycoprotein and its interaction, in Proceedings of the international symposium on serum albumin and alpha1-acid glycoprotein (Otagiri, M., Sugiyama, Y., Testa, B., and Tillement, J. P., Eds.) pp 45−54, Tokyo Print, Kumamoto, Japan.
13. Rojo-Dominguez, A., and Hernandez-Arana, A. (1993) Three-dimensional modeling of the protein moiety of human alpha1-acid glycoprotein, a lipocalin-family member. *Protein Seq. Data Anal. 5*, 349–355.
14. Kopecký, V. Jr., Ettrich, R., Hofbauerová, K., and Baumruk, V. (2003) Structure of human alpha1-acid glycoprotein and its high-affinity binding site. *Biochem. Biophys. Res. Commun. 300*, 41–46.
15. Zhu, F., Isaacs, N. W., Hecht, L., and Barron, L. D. (2005) Polypeptide and carbohydrate structure of an intact glycoprotein from Raman optical activity. *J. Am. Chem. Soc. 127*, 6142–6143.
16. Fasman, G. R. (1996) Circular dichroism and the conformational analysis of biomolecules , Plenum Press, New York.
17. Berova, N., Nakanishi, K., and Woody, R. W. (2000) Circular dichroism: principles and applications , 2nd ed., Wiley-VCH Press, New York.
18. Shanmugam, G., and Polavarapu, P. L. (2006) Structures of intact glycoproteins from vibrational circular dichroism. *Proteins 63*, 768–776.
19. Kabsch, W., and Sander, C. (1983) Dictionary of protein secondary structure: pattern recognition of hydrogen-bonded and geometric features. *Biopolymers 22*, 2577–2637.
20. King, S. M., and Johnson, W. C. (1999) Assigning secondary structure from protein coordinate data. *Proteins 35*, 313–320.
21. Sreerama, N., and Woody, R. W. (2000) Estimation of protein secondary structure from circular dichroism spectra: comparison of CONTIN, SELCON, and CDSSTR methods with an expanded reference set. *Anal. Biochem. 287*, 252–260.
22. Sreerama, N., Venyaminov, S. Y., and Woody, R. W. (1999) Estimation of the number of alpha-helical and beta-strand segments in proteins using circular dichroism spectroscopy. *Protein Sci. 8*, 370–380.
23. Toumadje, A., Alcorn, S. W., and Johnson, W. C. Jr. (1992) Extending CD spectra of proteins to 168 nm improves the analysis for secondary structures. *Anal. Biochem. 200*, 321–331.
24. Sutherland, J. C., Emrick, A., France, L. L., Monteleone, D. C., and Trunk, J. (1992) Circular dichroism user facility at the National Synchrotron Light Source: estimation of protein secondary structure. *BioTechniques 13*, 588–590.
25. Wallace, B. A., and Janes, R. W. (2001) Synchrotron radiation circular dichroism spectroscopy of proteins: secondary structure, fold recognition and structural genomics. *Curr. Opin. Chem. Biol. 5*, 567–571.
26. Ojima, N., Sakai, K., Matsuo, K., Matsui, T., Fukazawa, T., Namatame, H., Taniguchi, M., and Gekko, K. (2001) Vacuum-ultraviolet circular dichroism spectrophotometer using synchrotron radiation: optical system and on-line performance. *Chem. Lett. 30*, 522–523.
27. Matsuo, K., Sakai, K., Matsushima, Y., Fukuyama, T., and Gekko, K. (2003) Optical cell with a temperature-control unit for a vacuum-ultraviolet circular dichroism spectrophotometer. *Anal. Sci. 19*, 129–132.
28. Matsuo, K., Yonehara, R., and Gekko, K. (2004) Secondary-structure analysis of proteins by vacuum-ultraviolet circular dichroism spectroscopy. *J. Biochem. 135*, 405–411.
29. Matsuo, K., Yonehara, R., and Gekko, K. (2005) Improved estimation of the secondary structures of proteins by vacuum-ultraviolet circular dichroism spectroscopy. *J. Biochem. 138*, 79–88.
30. Matsuo, K, Watanabe, H., and Gekko, K. (2008) Improved sequence-based prediction of protein secondary structures by combining vacuum-ultraviolet circular dichroism spectroscopy with neural network. *Proteins 73*, 104–112.
31. Matsuo, K., Watanabe, H., Tate, S., Tachibana, H., and Gekko, K. (2009) Comprehensive secondary-structure analysis of disulfide variants of lysozyme by synchrotron-radiation vacuum-ultraviolet circular dichroism. *Proteins 77*, 191–201.
32. Lala, A. K., Kaul, P., and Ratnam, P. B. (1995) Membrane-protein interaction and the molten globule state: interaction of alpha-lactalbumin with membranes. *J. Protein Chem. 14*, 601–609.
33. Jones, D. T. (1999) Protein secondary structure prediction based on position-specific scoring matrices. *J. Mol. Biol. 292*, 195–202.
34. Bernstein, F. C., Koetzle, T. F., Williams, G. J. B., Meyer, E. F. Jr., Brice, M. D., Rodgers, J. R., Kennard, O., Shimanouchi, T., and Tasumi, M. (1977) The Protein Data Bank. A computer-based archival file for macromolecular structures. *J. Mol. Biol. 112*, 535–542.
35. Zell, A., Mamier, G., Vogt, M., Mache, N., Hubner, R., Doring, S., Herrmann, K. W., Soyez, T., Schmalzl, M., Sommer, T., Hatzigeorgiou, A., Posselt, D., Schreiner, T., Kett, B., Clemente, G., and Wieland, J. (1995) Stuttgart neural network simulator, Version 4.2, University of Stuttgart, Stuttgart, Germany (http://www.informatik.uni-stuttgart.de/ipvr/bv/projekte/snns/User Manual/UserManual.html).
36. Marti-Renom, M. A., Stuart, A. C., Fiser, A., Sánchez, R., Melo, F., and Sali, A. (2000) Comparative protein structure modeling of genes and genomes. *Annu. Rev. Biophys. Biomol. Struct. 29*, 291–325.
37. Laskowski, R. A., MacArthur, M. W., Moss, D. S., and Thornton, J. M. (1993) PROCHECK: a program to check the stereochemical quality of protein structures. *J. Appl. Crystallogr. 26*, 283–291.
38. Matsuo, K., and Gekko, K. (2004) Vacuum-ultraviolet circular dichroism study of saccharides by synchrotron radiation spectroscopy. *Carbohydr. Res. 339*, 591–597.
39. Aubert, J. P., and Loucheux-Lefebvre, M. H. (1976) Conformational study of alpha1-acid glycoprotein. *Arch. Biochem. Biophys. 175*, 400–409.
40. Matsuo, K., Namatame, H., Taniguchi, M., and Gekko, K. (2009) Vacuum-ultraviolet circular dichroism analysis of glycosaminoglycans by synchrotron-radiation spectroscopy. *Biosci., Biotechnol., Biochem. 73*, 557–561.
41. Stevens, E. S. (1986) Vacuum UV circular dichroism of polysaccharides. *Photochem. Photobiol. 44*, 287–293.
42. Pancoska, P., Janota, V., and Keiderling, T. A. (1999) Novel matrix descriptor for secondary structure segments in proteins: demonstration of predictability from circular dichroism spectra. *Anal. Biochem. 267*, 72–83.
43. Adamczak, R., Porollo, A., and Meller, J. (2005) Combining prediction of secondary structure and solvent accessibility in proteins. *Proteins 59*, 467–475.
44. Wood, M. J., and Hirst, J. D. (2005) Protein secondary structure prediction with dihedral angles. *Proteins 59*, 476–481.
45. Bondugula, R., and Xu, D. (2007) MUPRED: a tool for bridging the gap between template based methods and sequence profile based

methods for protein secondary structure prediction. *Proteins 66*, 664–670.
46. Cornell, D. G., and Patterson, D. L. (1989) Interaction of phospholipids in monolayers with beta-lactoglobulin adsorbed from solution. *J. Agric. Food Chem. 37*, 1455–1459.
47. Van der Goot, F. G., González-Mañas, J. M., Lakey, J. H., and Pattus, F. (1991) A "molten-globule" membrane-insertion intermediate of the pore-forming domain of colicin A. *Nature 354*, 408–410.
48. Gasymov, O. K., Abduragimov, A. R., Yusifov, T. N., and Glasgow, B. J. (1998) Structural changes in human tear lipocalins associated with lipid binding. *Biochim. Biophys. Acta 1386*, 145–156.
49. Nishi, K., Komine, Y., Sakai, N., Maruyama, T., and Otagiri, M. (2005) Cooperative effect of hydrophobic and electrostatic forces on alcohol-induced alpha-helix formation of alpha1-acid glycoprotein. *FEBS Lett. 579*, 3596–3600.
50. Rost, B., Fariselli, P., and Casadio, R. (1996) Topology prediction for helical transmembrane proteins at 86% accuracy. *Protein Sci. 5*, 1704–1718.
51. Hirokawa, T., Boon-Chieng, S., and Mitaku, S. (1998) SOSUI: classification and secondary structure prediction system for membrane proteins. *Bioinformatics 14*, 378–379.
52. Everett, J. K. Helical wheel drawing program, Center for Advanced Biotechnology and Medicine, New Jersey (http://www-nmr.cabm.rutgers.edu/bioinformatics/ Proteomic_tools/Helical _wheel/).
53. Nishi, K., Komine, Y., Fukunaga, N., Maruyama, T., Suenaga, A., and Otagiri, M. (2006) Involvement of disulfide bonds and histidine 172 in a unique beta-sheet to alpha-helix transition of alpha 1-acid glycoprotein at the biomembrane interface. *Proteins 63*, 611–620.
54. Yamamoto, T., Izumi, S., and Gekko, K. (2004) Mass spectrometry on hydrogen/deuterium exchange of dihydrofolate reductase: effects of ligand binding. *J. Biochem. 135*, 663–671.